All-Optical Hybrid VO_2/Si Waveguide Absorption Switch at Telecommunication Wavelengths

Jorge Parra, *Student Member, IEEE,* Todora Ivanova, Mariela Menghini, Pía Homm, Jean-Pierre Locquet, and Pablo Sanchis, *Senior Member, IEEE*

***Abstract*—Vanadium dioxide (VO_2) is one of the most promising materials for developing hybrid photonic integrated circuits (PICs). At telecommunication wavelengths, VO_2 exhibits a large change on the refractive index ($\Delta n \sim 1$ and $\Delta \kappa \sim 2.5$) between its insulating and metallic state. Such insulating-to-metal transition (IMT) can be triggered by light, which could enable all-optical hybrid VO_2-waveguide devices. Here, we experimentally demonstrate an all-optical absorption switch using a hybrid VO_2/Si waveguide fully compatible with the silicon photonics platform. All-optical characterization was carried out for TE polarization and at telecommunication wavelengths using an in-plane approach. The temporal dynamics were retrieved by using pump-probe measurements. Our results show an extinction ratio of 0.7 dB/μm with a maximum switchable length of 15 μm, a switching speed as low as 318 ns and an energy per switch of 15.8 nJ. The inherit large optical bandwith of a non-resonant waveguide poses this device as a promising candidate for developing all-optical and broadband silicon PICs.**

***Index Terms*—optical switching, photonic integration, vanadium dioxide, silicon photonics.**

I. Introduction

PHASE change materials (PCMs) present unique optical properties that can be tuned by external stimuli [1]. Among them, vanadium dioxide (VO_2) is a complementary metal-oxide-semiconductor (CMOS)-compatible material that exhibits a reversible and hysteretic insulating-to-metal transition (IMT) [2], [3]. Such IMT can be induced with different external stimuli such as temperature [4], electric field [5], [6] or optical excitation [7]. More than 10^{10} switching cycles have been demonstrated in VO_2 by electrical triggering [8].

Regarding the optical properties, the phase transition of VO_2 it is accompanied with a significant change of the complex refractive index at telecom wavelengths [9]. This large difference in both real and imaginary parts has been exploited in the silicon (Si) photonics platform for proposing and developing ultra-compact hybrid VO_2/Si devices [9]–[30]. Most of the experimental works exploit the near room temperature value in which the IMT occurs (~ 65 ºC) by placing a microheater near the hybrid waveguide. In this way, large optical extinction ratios (> 1 dB/μm) with few microseconds of switching speed have been obtained [12]–[15]. Electrical triggering by applying an electric field between two metal electrodes has also been demonstrated in hybrid VO_2/Si devices [21], [22]. A fast field-driven switching in the nanosecond range initiating the IMT was observed. However, a slower current-driven mechanism based on Joule heating was necessary for a full VO_2 transition and so maximizing the extinction ratio.

Besides electrical triggering, optical excitation has been widely employed to investigate the VO_2 phase transition on thin-film structures and ultra-fast switching times as fast as femtoseconds have been achieved [7], [28], [31]–[36]. More recently, experimental demonstration of all-optical VO_2-waveguide devices have been reported [26]–[28], [37]. However, experiments were carried out in a similar way to those focusing on the process behind the photo-induced phase transition of VO_2 using free-space pump-probe studies.

A comparison with previous experimental work is summarized in Table I in terms of key parameters such as wavelength, switching energy and optical loss. Note that, in previous work, the pump or control signal is not waveguided within the chip but out-of-plane and/or its wavelength is out of the transparent region of silicon (1.1–7 μm). The free-space configuration is prone to attain low both power (few microwatts) and switching energies (few picojoules) [27] since the light directly impinges into the whole VO_2 layer. Conversely, in a waveguide approach, similar switching energies can only be achieved by increasing the power in order to compensate: (i) the exponential attenuation that suffers the light through the hybrid waveguide; and (ii) the low fraction of optical mode that interacts with the VO_2. In [37], Wong *et al.* obtained switching energies of few picojoules using a SiN waveguide but at the expenses of guiding a high peak power, which is unfeasible in silicon due to nonlinear effects [38]. On the other hand, in out-of-plane configurations, switching times range from few picoseconds to several seconds mainly due to the different optical pumping scheme and device structure. However, such investigation has not been carried out using evanescent coupling with a practical on-chip implementation.

Here, an all-optical absorption switch using a hybrid VO_2/Si waveguide is demonstrated. All-optical switching is achieved by an in-plane optical pumping excitation at telecom wavelengths, thus providing a device fully compatible with current silicon photonic integrated circuits (PICs). Moreover, a stable

This work was supported by Ministerio de Economía y Competitividad (MINECO) (TEC2016-76849); Ministerio de Ciencia e Innovación (PID2019-111460GB-I00, FPU17/04224); Generalitat Valenciana (PROMETEO/2019/123).

J. Parra, T. Ivanova and P. Sanchis* are with the Nanophotonics Technology Center, Universitat Politècnica de València, 46022 Valencia, Spain (* Corresponding author e-mail: pabsanki@ntc.upv.es).

M. Menghini was with the Department of Physics and Anstronomy, KU Leuven, Celestijnenlaan 200D, 3001 Leuven, Belgium. Currently, she is with IMDEA Nanociencia, Calle Faraday 9, E28049, Madrid, Spain.

P. Homm was with the Department of Physics and Anstronomy, KU Leuven, Celestijnenlaan 200D, 3001 Leuven, Belgium.

J.-P. Locquet is with the Department of Physics and Anstronomy, KU Leuven, Celestijnenlaan 200D, 3001 Leuven, Belgium.

Manuscript received -; revised -.

TABLE I. Comparison of Experimental All-Optical VO_2-Waveguide Devices.

Ref.	Platform	Pump configuration	Pump wavelength (nm)	Switching time	Switching energy	Peak power	Polarization	Insertion loss (dB/μm)	Extinction ratio (dB/μm)
[26]	Si	Out-of-plane	532	~ 180 s	15 μJ*	84 nW†	TE	–	–§
[27]	Si	Out-of-plane	1064	$\sim 0.01-1$ μs	3 pJ*	120 μW†	–	2	4
[28]	Si	Out-of-plane	1670	~ 1 ps	32 pJ*	–	–	–	2
[37]	SiN	In-plane	$700-1000$	–	6.4 pJ	45 W‡	TM	0.98	1.68
This work	Si	In-plane	1560	$\sim 0.1-1$ μs	15.8 nJ	13.2 mW	TE	0.91	0.7

Polarization, insertion loss and extinction ratio are given at $\lambda = 1550$ nm. Except Ref. [27] that is at an unknown wavelength between 1500 and 1600 nm.
* Estimated from the given value of fluence and VO_2 area on top of the waveguide in the reference, i.e., Energy = Fluence × VO_2 area.
† Derived from the values of fluence, pulse width and VO_2 area on top of the waveguide given in the reference, i.e., Power $= \frac{\text{Fluence} \times VO_2 \text{ area}}{\text{Pulse width}}$.
‡ Estimated from the values of energy and pulse width (140 fs) given in the paper as Power $= \frac{\text{Energy}}{\text{Pulse width}}$.
§ Could not be estimated. An extinction ratio of 10 dB was reported but using a ring device.

and long-term operation is expected by protecting the VO_2 from the external environment by using a SiO_2 cladding [39], [40].

The paper is organized as follows. In Section II, the VO_2 and transmission response of the hybrid waveguide are characterized and compared with simulations. Then, in Section III, the static and temporal all-optical response of the switch is experimentally demonstrated and analyzed. Finally, conclusions and potential applications are drawn in Section IV.

II. The Hybrid VO_2/Si Waveguide

A. Fabrication

The fabricated hybrid VO_2/Si waveguide used in this work is shown in Fig. 1a. This comprises a Si waveguide with a 20-μm-long VO_2 patch on top. A scheme of the cross-section is depicted in Fig. 1b. The Si waveguide is 480 nm × 220 nm to work in the single-mode region. A 50-nm-thick SiN layer is used for planarization of the silicon surface. Between the silicon waveguide and the SiN layer there is a 10-nm-thick of oxide. A 40-nm-thick VO_2 layer is placed atop of the SiN layer. The VO_2 layer was formed by growing a VO_x layer by molecular beam epitaxy (MBE) followed by an ex-situ post-annealing at 400 °C in forming gas [4]. Finally, a 700-nm-thick SiO_2 upper-cladding was deposited by plasma-enhanced chemical vapor deposition (PECVD) to avoid oxidation of the VO_2 due to environmental variations.

B. VO_2 Optical Characterization

Spectroscopic ellipsometry measurements were carried out on a dummy Si sample with the same 40-nm-thick VO_2 at room temperature (RT) and 100 °C by using a hot plate to determine the VO_2 refractive index both in the insulating and metallic state. These measurements were performed before and after depositing the SiO_2 cladding to check for possible variations in the refractive index of the VO_2 due to this processing step. The refractive index is almost not affected in the metallic state, as shown in Fig. 2a, whereas a small variation can be observed in the insulating state. Nevertheless, the hysteresis in the VO_2 phase transition is preserved as depicted in Fig. 2b, where the phase of the VO_2 refractive index with the temperature is shown during a heating-cooling

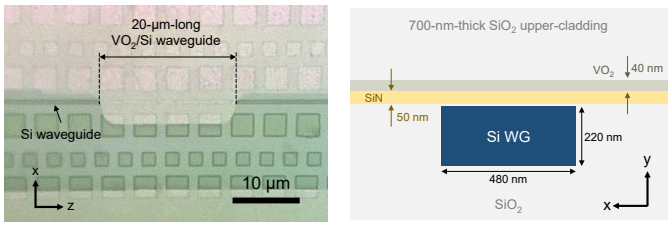

(a) (b)

Fig. 1. (a) Optical image of the fabricated hybrid 20-μm-long VO_2/Si waveguide before depositing the SiO_2 upper-cladding. The silicon squares shown in the image are used for the planarization process. (b) Cross-section scheme of the hybrid waveguide.

cycle at $\lambda = 1550$ nm. For both claddings, the IMT begins around 60 °C and the refractive index varied from $2.74 + j0.5$ (insulating) to $1.78 + j2.58$ (metallic) for the SiO_2 cladding.

C. Simulated Transmission Response

Based on the aforementioned VO_2 refractive index values, finite element method (FEM) simulations were carried out to obtain the effective refractive index, $n_{\text{eff}} + j\kappa_{\text{eff}}$, of the guides modes for TE polarization. Due to the absorptive behavior of the switch, we will only work with the imaginary part. From this, the propagation loss, α, for both VO_2 states can be calculated following the well-known expression:

$$\alpha = 20 \log_{10}(e) \frac{2\pi}{\lambda} \kappa_{\text{eff}}. \quad (1)$$

The resulting propagation losses are shown in Fig. 3a for wavelength values covering the C- and L-band. In the insulating state, propagation losses are around 0.7 dB/μm and remain independent of the wavelength due to the flat response of the VO_2 refractive index as shown in Fig. 2a. For the metallic state, propagation losses range from 1.2 dB/μm to almost 2 dB/μm from 1500 to 1650 nm, leading to an extinction ratio between 0.5 and 1.1 dB/μm. Nonetheless, a switch with the aim of covering both bands and with a required minimum extinction ratio would be feasible since it would be designed only taking into account the limiting C-band. Therefore, this kind of all-optical switch based on

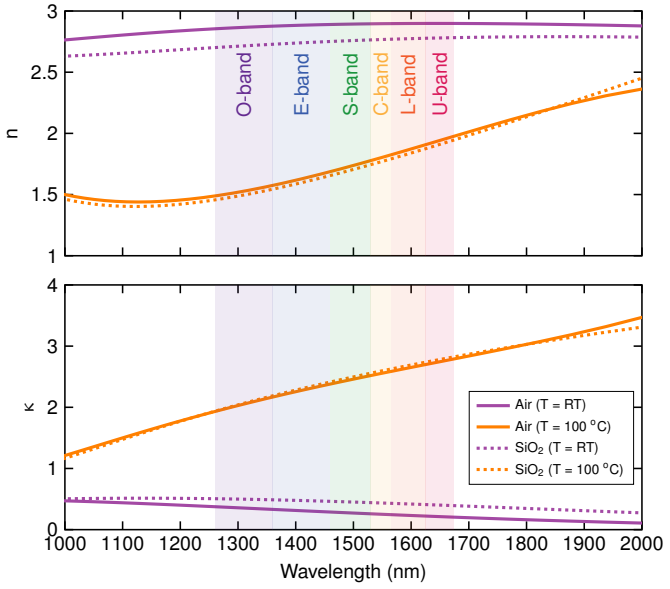

(a)

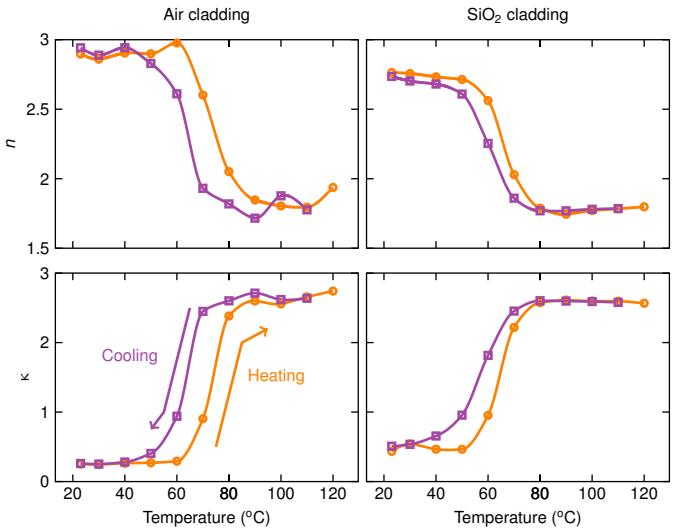

(b)

Fig. 2. Refractive indices of VO_2 obtained by spectroscopic ellipsometry with an air and SiO_2 cladding: (a) as a function of the wavelength for the insulating (T = RT) and metallic (T = 100 °C) states; and (b) at $\lambda = 1550$ nm as a function of the temperature during a heating-cooling cycle.

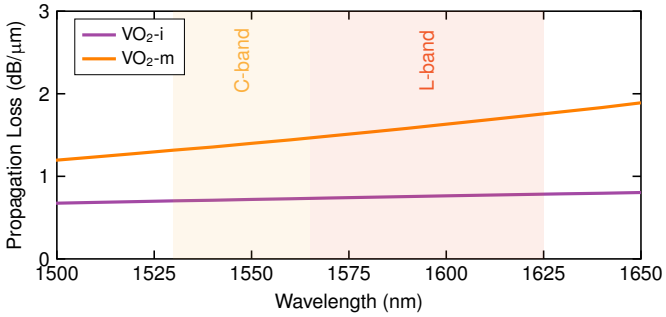

(a)

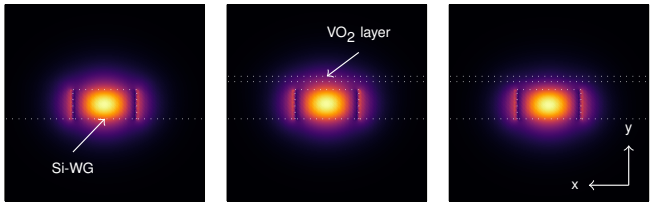

(b) (c) (d)

Fig. 3. (a) Simulated propagation loss as a function of the wavelength for the VO_2 in the insulating (VO_2-i) and metallic (VO_2-m) state. Normalized electric field (E_x) of the silicon waveguide (b) without VO_2 and with the VO_2 layer in the (c) insulating and (d) metallic state at $\lambda = 1550$ nm. Simulations were carried out for TE polarization and using the VO_2 refractive index values given in Fig. 2a.

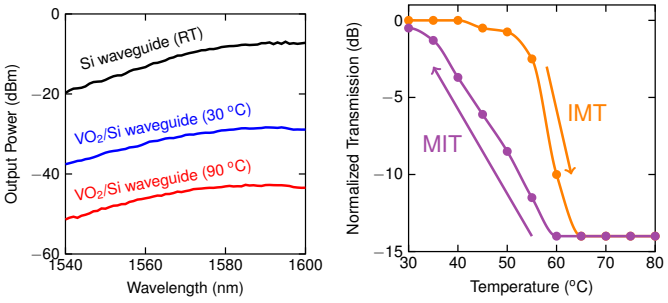

(a) (b)

Fig. 4. (a) Spectra of a reference silicon waveguide and the hybrid waveguide in the insulating (T = 30 °C) and metallic (T = 90 °C) states. Laser output power was 0 dBm. (b) Normalized transmission of the hybrid waveguide as a function of the temperature for a heating-cooling cycle at $\lambda = 1550$ nm.

non-resonant structure would be ultra-broadband. On the other hand, the optical mode of the silicon waveguide without the VO_2 capping (Fig. 3b) is very similar with those of the VO_2/Si waveguide in the insulating and metallic state as depicted in Figs. 3c and 3d, respectively. Therefore, optical losses due to mode mismatch between the silicon and the hybrid waveguide are expected to be much lower in comparison with propagation losses.

Larger extinction ratios could be obtained by using TM polarization and exploiting the formation of a high-lossy hybrid plasmonic mode in the metallic state [16]. Our simulations predict an increase of the extinction ratio up to 6.71 dB/μm at 1550 nm. However, propagation loss in the insulating state increases to 1.45 dB/μm and there is a higher mode mismatch that could give rise to larger coupling losses. Moreover, TM is not the most widely used polarization in silicon photonics due to the lower optical confinement.

D. Experimental Transmission Response

The spectrum of the hybrid waveguide was measured with the VO_2 in the insulating and metallic state (Fig. 4a). To this end, the temperature of the chip was set at 30 °C and 90 °C, respectively, by using a Peltier device. Light was

coupled to/from the chip by means of TE grating couplers. A reference waveguide without VO_2 was also measured to estimate grating and VO_2 losses. Experimental optical loss of VO_2 in the insulating and metallic state was 18.2 dB and 32.2 dB, respectively, which delivered an extinction ratio of 14 dB, in fair agreement with the values of propagation loss given by simulations. Moreover, these values would confirm the low losses due to the optical mode mismatch between the silicon waveguide and the device.

The typical hysteretic response of VO_2 on its optical loss was obtained upon a heating-cooling cycle (Fig. 4b). On one hand, the IMT occurred around 58 ^{o}C in a window between 55 ^{o}C and 63 ^{o}C. On the other hand, the metal-to-insulating transition (MIT) started at 60 ^{o}C and finished around 30 ^{o}C.

III. All-Optical Switching

A. Static Switching Response

Prior to temporal measurements, the all-optical static response of the hybrid waveguide was investigated. The transmission of the waveguide was collected as a function of the input power. A tunable continuous-wave (CW) laser with an erbium-doped fiber-amplifier (EDFA) was used to generate high power optical signals to drive the VO_2 into the metallic state. The normalized transmission as a function of the input power at the facet of the hybrid waveguide is shown in Fig. 5a. The power at the facet is calculated by subtracting the output power delivered by the EDFA to the grating estimated loss from the Si reference waveguide (see Fig. 4a). Several optical cycles were performed varying the maximum power. On one hand, a hysteresis is observed for all the cycles, which confirms that optical loss is due to the metallic/insulating change of the VO_2. On the other hand, the loss is proportional to the input power. This indicates that only a portion of the VO_2 patch becomes metallic and it is attributed to the attenuation that experiences the optical signal due to the VO_2 absorption.

Based on these measurements and the simulated optical loss, the VO_2 underwent the metallic state with a rate of 1.06 μm/dBm for input powers higher than 3.5 dBm (Fig. 5b). To change the 20-μm-long VO_2 on top of the waveguide, an optical power of 22.4 dBm would be necessary at the facet. It is important to take into account that in the static regime the IMT is triggered by photo-thermal excitation [26]. Hence, the VO_2 could be damaged or permanently changed to another phase like V_2O_5 if this surpasses 600 ^{o}C [41]. In our hybrid waveguide, a permanent change was obtained when the input power was increased up to 18 dBm ($\sim$ 15 μm of metallic VO_2). A larger insertion loss was measured while a degradation in a fragment of the VO_2 layer was also observed by optical inspection. Furthermore, the response showed in Fig. 5a could not be replicated using the same input powers.

B. Temporal Switching Dynamics

Based on the all-optical static measurements and constraints, the temporal dynamics of the hybrid waveguide were investigated. To this end, the temporal characteristics were obtained from the hybrid waveguide transmission using a pump-probe technique in the telecom wavelength region. Small peak powers and short pulses were used to avoid damaging of the VO_2 layer. Thus, a small fragment of VO_2 underwent the metallic state. Temporal measurements were stable during the entire characterization process.

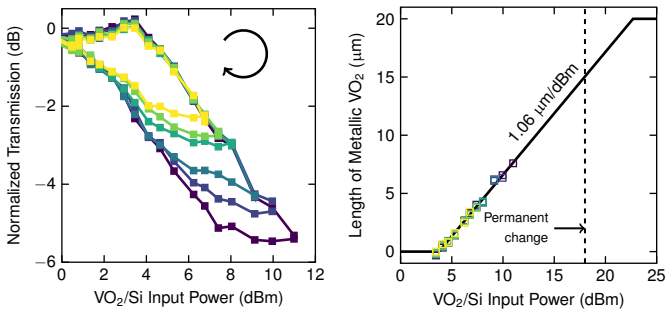

(a) (b)

Fig. 5. (a) Normalized transmission as a function of the optical power. Different optical cycles were performed varying the maximum power. The arrow indicates the direction of the cycle. (b) Fragment of VO_2 in the metallic state as a function of the optical power from experimental results (square markers) and fitting (solid line). For both figures, optical power is given at the facet of the hybrid waveguide and $\lambda = 1550$ nm.

The set-up used for this work is schemed in Fig. 6. On one hand, the probe signal was generated by using a CW laser at 1550 nm with an output power of 3 dBm and set to TE polarization with a 3-paddle manual polarization rotator (PR). On the other hand, the pump pulses were generated from a CW laser at 1560 nm with an output power of 5 dBm together with an external electro-optic modulator (EOM) and an arbitrary waveform generator. The output of the EOM was amplified with an EDFA. Then, the high-power pump signal was TE-polarized with another PR and filtered in order to remove the noise introduced by the EDFA. The removal of the spectral power coming from ASE noise is necessary to avoid any possible residual heat. Such heat might have influence on the switching performance and prevent the full recovery of the VO_2 insulating state. Before injecting the probe and pump signals to the chip, both were combined using a 3 dB directional coupler. The output of the chip was filtered to remove the pump signal, amplified with another EDFA to compensate chip optical loss, and filtered again to remove the EDFA noise. Finally, the temporal response was recorded by means of a high-speed photodiode and an oscilloscope.

A 50-μs-wide rectangular pulse with a repetition rate of 10 kHz was generated. The amplitude of the pump signal was set to obtain around 8 dBm at the facet of the hybrid waveguide. This lead to a energy consumption of 315 nJ. The normalized output is shown in Fig. 7a. Upon the pump signal, the probe suffered a drop on its power in good agreement with the results obtained in the static measurements (see Fig. 5a). The drop of the probe (OFF state) is associated with the high-loss metallic state of the VO_2, whereas the recovery (ON state) is linked to the low-loss insulating one. The switching

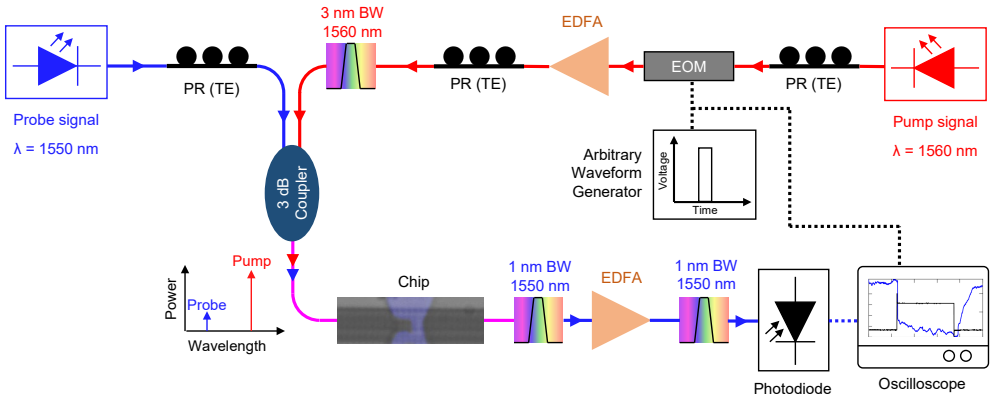

Fig. 6. Schematic of the experimental set-up used for testing the all-optical temporal response of the hybrid VO_2/Si waveguide. In the chip image, the VO_2 in the insulating state is false colored in blue.

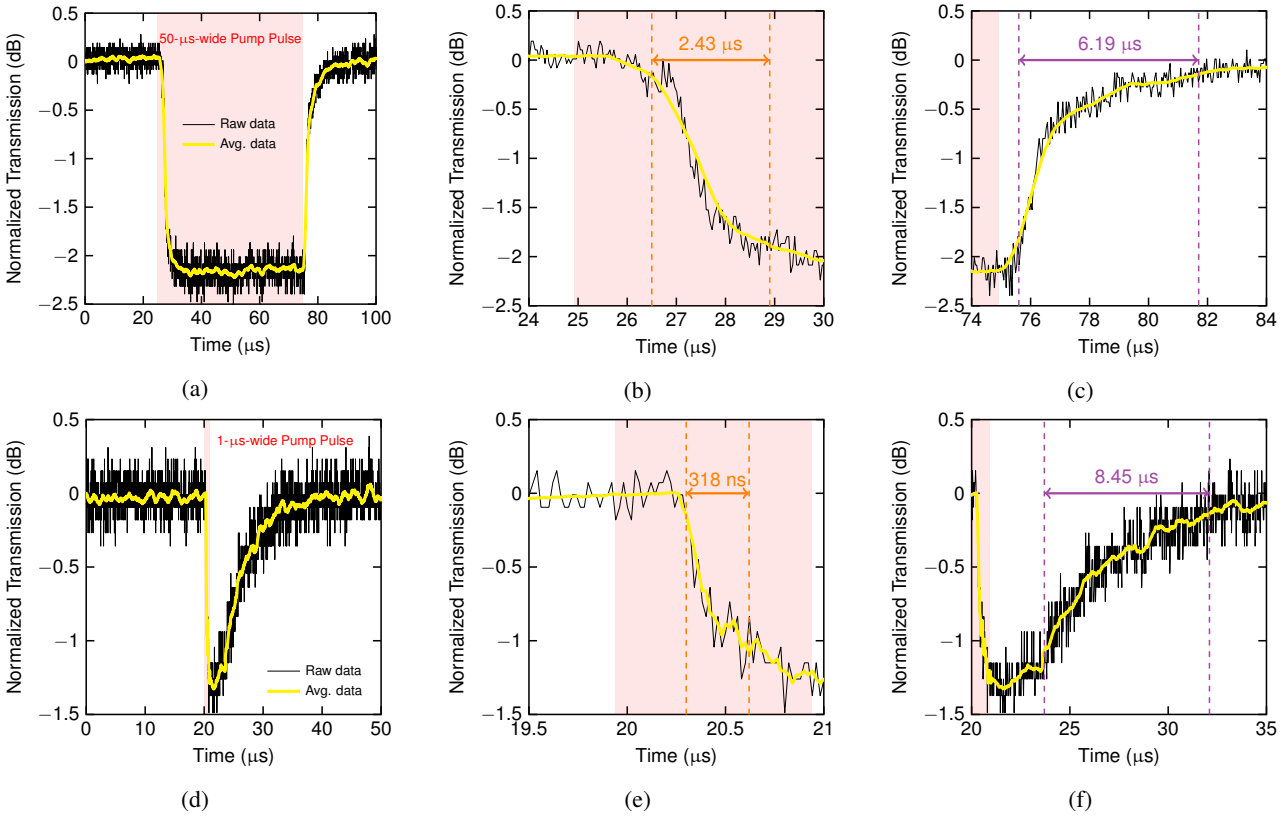

Fig. 7. Normalized output of the probe signal as a function of the time upon: (a-c) 50-μs-wide and 8 dBm rectangular pump pulse and (d-f) 1-μs-wide and 12 dBm rectangular pump pulse. (b,c) and (e,f) are the zooms of fall and rise times for (a) and (d), respectively. Results are given at 1550 nm and 1560 nm for the probe and pump signals, respectively. The pump power values are at the facet of the hybrid waveguide. The time in which the pump signal is applied is highlighted in light red.

times were obtained from the averaged data and following the 10%-90% rule. A value of 2.43 μs (Fig. 7b) and 6.19 μs (Fig. 7c) was obtained for the OFF and ON states, respectively. The difference between both values is attributed to the thermal increment required to complete the IMT and MIT of the VO_2 (see Fig. 4b). The longer switch time of the ON state is due to the fact the MIT needs a wider switching window compared to the IMT (OFF state) to complete the phase transition. This difference in the steepness between the IMT and MIT, being the first more abrupt, has also been reported in previous work [9] and it is attributed to different crystal grain sizes during the structural phase transition [42].

The timescales suggest a photo-thermal effect behind the VO_2. Notably, switching times are in the same order of magnitude to those reported using microheaters [14]. Therefore, the switching mechanism is attributed to be of thermal origin. On one hand, the insulating to metal switching (OFF switching) is due to the fact of heat arising from the VO_2 optical absorption.

On the other hand, the metal to insulating switching (ON switching) involves a thermal dissipation process.

The temporal response of the device is thus conditioned by the surrounding materials as in thermo-optic phase shifters [43]–[45]. Nevertheless, the nonlinear thermal temporal response of VO_2 can be taken in advantage to reduce the insulating to metal switching times while maintaining the extinction ratio. To this end, higher optical pump powers should be used together with a drastic shortening of the pulse width. The first, to increase the heating rate, while the second to avoid the VO_2 thermal damage threshold. To prove this point, the pulse width was 50 times decreased to 1 μs whereas the pump power was only increased 2.5 times up to 12 dBm. These values were chosen with the aim of achieving a similar extinction ratio. The normalized temporal response is shown in Fig. 7d. The switching time of insulating to metal was reduced one order of magnitude down to 318 ns (Fig. 7e). This reduction is attributed to the higher heating rate, which was confirmed by observing the delay between the pump and the actual switch of the probe. For this latter case, the delay was reduced from around 1.5 μs (Fig. 7b) to 300 ns (Fig. 7e). On the other hand, the metal to insulating switching time remained at a similar value (Fig. 7f), since it basically depends on the thermal dissipation rate of the structure [21], [22]. Furthermore, the non-proportional shortening of the pulse width with the power increase leads to a reduction of the energy consumption, being for this case one order of magnitude lower and achieving 15.8 nJ.

As a consequence, the all-optical hybrid VO_2/Si device using an in-plane approach is governed by thermal conductive dynamics. The switching time from insulating to metal state could be reduced by increasing the pump power while reducing the pump pulse, which also benefits of achieving lower energy consumption values. On the other hand, reducing the size of the VO_2 patch [27] or including a heat sink, i.e., a high thermal conductive material close to the VO_2 layer, would reduce the heating/cooling time, thus yielding to faster switching speeds.

IV. Conclusions

In conclusion, we have experimentally demonstrated an all-optical absorption switch using a hybrid VO_2/Si waveguide. On one hand, all-optical static results show an extinction ratio of 0.7 dB/μm with a maximum switchable length of 15 μm. This value is limited by the maximum temperature that can achieve the VO_2 without suffering a permanent and irreversible change. On the other hand, insertion loss could be reduced by using a granular morphology on the VO_2 layer [13]. Another pathway that could lead to a further reduction with high extinction ratio would be the utilization of a directional coupler [18], [46], [47]. By this way, the insertion loss would be minimized by designing the directional coupler to switch between the bar and cross states when the VO_2 changes from insulating to the metallic state. All-optical switching results show that the temporal dynamics of this device are thermal, in which the heat arises from the light absorbed by the VO_2. Switching values in the nano and microsecond range have been obtained with energy consumptions as low as nanojoules.

All-optical switching in VO_2/Si technology may be used in applications requiring a nonlinear optical response. Parallel computing architectures such as neuromorphics could use VO_2/Si switches for performing activation or nonlinear threshold functions [48]. Furthermore, due to the broad optical response, VO_2/Si switches could be used in parallel photonic circuits based on wavelength division multiplexing such as photonic tensor cores [49], [50].

Acknowledgment

The authors thank David Zurita for his help with the experimental set-up, and Maria Recaman for her inputs with VO_2.

References

[1] F. J. Morin, "Oxides which show a metal-to-insulator transition at the neel temperature," *Physical Review Letters*, vol. 3, no. 1, pp. 34–36, 1959.

[2] K. Liu, S. Lee, S. Yang, O. Delaire, and J. Wu, "Recent progresses on physics and applications of vanadium dioxide," *Materials Today*, vol. 21, no. 8, pp. 875–896, 2018.

[3] S. Cueff, J. John, Z. Zhang, J. Parra, J. Sun, R. Orobtchouk, S. Ramanathan, and P. Sanchis, "VO2 nanophotonics," *APL Photonics*, vol. 5, no. 11, p. 110901, 2020.

[4] B. Van Bilzen, P. Homm, L. Dillemans, C. Y. Su, M. Menghini, M. Sousa, C. Marchiori, L. Zhang, J. W. Seo, and J. P. Locquet, "Production of VO2 thin films through post-deposition annealing of V2O3 and VOx films," *Thin Solid Films*, vol. 591, pp. 143–148, 2015.

[5] B. G. Chae, H. T. Kim, D. H. Youn, and K. Y. Kang, "Abrupt metal-insulator transition observed in VO2 thin films induced by a switching voltage pulse," *Physica B: Condensed Matter*, vol. 369, no. 1-4, pp. 76–80, 2005.

[6] C. Ko and S. Ramanathan, "Observation of electric field-assisted phase transition in thin film vanadium oxide in a metal-oxide-semiconductor device geometry," *Applied Physics Letters*, vol. 93, no. 25, pp. 1–4, 2008.

[7] M. F. Becker, A. B. Buckman, R. M. Walser, T. Lépine, P. Georges, and A. Brun, "Femtosecond laser excitation dynamics of the semiconductor-metal phase transition in VO2," *Journal of Applied Physics*, vol. 79, no. 5, pp. 2404–2408, 1996.

[8] I. P. Radu, B. Govoreanu, S. Mertens, X. Shi, M. Cantoro, M. Schaekers, M. Jurczak, S. De Gendt, A. Stesmans, J. A. Kittl, M. Heyns, and K. Martens, "Switching mechanism in two-terminal vanadium dioxide devices," *Nanotechnology*, vol. 26, no. 16, 2015.

[9] R. M. Briggs, I. M. Pryce, and H. A. Atwater, "Compact silicon photonic waveguide modulator based on the vanadium dioxide metal-insulator phase transition," *Optics Express*, vol. 18, no. 11, p. 11192, 2010.

[10] L. Sanchez, S. Lechago, A. Gutierrez, and P. Sanchis, "Analysis and Design Optimization of a Hybrid VO2/Silicon 2 x 2 Microring Switch," *IEEE Photonics Journal*, vol. 8, no. 2, 2016.

[11] L. Sánchez, A. Rosa, A. Griol, A. Gutierrez, P. Homm, B. Van Bilzen, M. Menghini, J. P. Locquet, and P. Sanchis, "Impact of the external resistance on the switching power consumption in VO2 nano gap junctions," *Applied Physics Letters*, vol. 111, no. 3, pp. 1–4, 2017.

[12] K. J. Miller, K. A. Hallman, R. F. Haglund, and S. M. Weiss, "Silicon waveguide optical switch with embedded phase change material," *Optics Express*, vol. 25, no. 22, p. 26527, 2017.

[13] I. Olivares, L. Sánchez, J. Parra, R. Larrea, A. Griol, M. Menghini, P. Homm, L.-W. Jang, B. van Bilzen, J. W. Seo, J.-P. Locquet, and P. Sanchis, "Optical switching in hybrid VO2/Si waveguides thermally triggered by lateral microheaters," *Optics Express*, vol. 26, no. 10, p. 12387, 2018.

[14] L. D. Sánchez, I. Olivares, J. Parra, M. Menghini, P. Homm, J.-P. Locquet, and P. Sanchis, "Experimental demonstration of a tunable transverse electric pass polarizer based on hybrid VO 2 /silicon technology," *Optics Letters*, vol. 43, no. 15, p. 3650, 2018.

[15] V. Jeyaselvan, A. Pal, P. S. Anil Kumar, and S. K. Selvaraja, "Thermally-induced optical modulation in a vanadium dioxide-on-silicon waveguide," *OSA Continuum*, vol. 3, no. 1, p. 132, 2020.

[16] K. Shibuya, Y. Atsumi, T. Yoshida, Y. Sakakibara, M. Mori, and A. Sawa, "Silicon waveguide optical modulator driven by metal–insulator transition of vanadium dioxide cladding layer," *Optics Express*, vol. 27, no. 4, p. 4147, 2019.

[17] M. Sadeghi, B. Janjan, M. Heidari, and D. Abbott, "Mid-infrared hybrid Si/VO2 modulator electrically driven by graphene electrodes," *Optics Express*, vol. 28, no. 7, p. 9198, 2020.

[18] J. T. Kim, "CMOS-compatible hybrid plasmonic modulator based on vanadium dioxide insulator-metal phase transition," *Optics Letters*, vol. 39, no. 13, p. 3997, 2014.

[19] J. H. Choe and J. T. Kim, "Design of vanadium dioxide-based plasmonic modulator for both TE and TM modes," *IEEE Photonics Technology Letters*, vol. 27, no. 5, pp. 514–517, 2015.

[20] P. Markov, K. Appavoo, R. F. Haglund, and S. M. Weiss, "Hybrid Si-VO2-Au optical modulator based on near-field plasmonic coupling," *Optics Express*, vol. 23, no. 5, p. 6878, 2015.

[21] P. Markov, R. E. Marvel, H. J. Conley, K. J. Miller, R. F. Haglund, and S. M. Weiss, "Optically Monitored Electrical Switching in VO2," *ACS Photonics*, vol. 2, no. 8, pp. 1175–1182, 2015.

[22] A. Joushaghani, J. Jeong, S. Paradis, D. Alain, J. Stewart Aitchison, and J. K. S. Poon, "Wavelength-size hybrid Si-VO_2 waveguide electroabsorption optical switches and photodetectors," *Optics Express*, vol. 23, no. 3, p. 3657, 2015.

[23] S. Based, V. O. Si, and H. S. Waveguides, "Design and Simulation of Compact Optical Modulators and Switches Based on Si-VO2-Si Horizontal Slot Waveguides," *Journal of Applied Physics*, vol. 35, no. 14, pp. 3020–3028, 2017.

[24] S. Mohammadi-Pouyan, M. Miri, and M. H. Sheikhi, "Design of a vanadium dioxide-based dual-polarization optical PAM4 modulator," *Journal of the Optical Society of America B*, vol. 35, no. 12, p. 3094, 2018.

[25] B. M. Younis, A. M. Heikal, M. Hussein, S. S. A. Obayya, and M. F. O. Hameed, "Hybrid Si-VO2 modulator with ultra-high extinction ratio based on slot TM mode," *Optics Express*, vol. 27, no. 26, p. 37454, 2019.

[26] J. D. Ryckman, V. Diez-Blanco, J. Nag, R. E. Marvel, B. K. Choi, R. F. Haglund, and S. M. Weiss, "Photothermal optical modulation of ultra-compact hybrid Si-VO_2 ring resonators," *Optics Express*, vol. 20, no. 12, p. 13215, 2012.

[27] J. D. Ryckman, K. A. Hallman, R. E. Marvel, R. F. Haglund, and S. M. Weiss, "Ultra-compact silicon photonic devices reconfigured by an optically induced semiconductor-to-metal transition," *Optics Express*, vol. 21, no. 9, p. 10753, 2013.

[28] R. F. Haglund, K. A. Hallman, K. J. Miller, and S. M. Weiss, "Picosecond Optical Switching in Silicon Photonics Using Phase-Changing Vanadium Dioxide," *2019 Conference on Lasers and Electro-Optics, CLEO 2019 - Proceedings*, vol. 1, pp. 2–3, 2019.

[29] L. Chen, H. Ye, Y. Liu, D. Wu, R. Ma, and Z. Yu, "Numerical investigations of an optical switch based on a silicon stripe waveguide embedded with vanadium dioxide layers," *Photonics Research*, vol. 5, no. 4, p. 335, 2017.

[30] J. K. Clark, Y. L. Ho, H. Matsui, and J. J. Delaunay, "Optically Pumped Hybrid Plasmonic-Photonic Waveguide Modulator Using the VO2 Metal-Insulator Phase Transition," *IEEE Photonics Journal*, vol. 10, no. 1, 2018.

[31] A. Cavalleri, C. Tóth, C. W. Siders, J. A. Squier, F. Ráksi, P. Forget, and J. C. Kieffer, "Femtosecond structural dynamics in VO2 during an ultrafast solid-solid phase transition," *Physical Review Letters*, vol. 87, no. 23, pp. 237 401–1–237 401–4, 2001.

[32] A. Cavalleri, T. Dekorsy, H. H. Chong, J. C. Kieffer, and R. W. Schoenlein, "Evidence for a structurally-driven insulator-to-metal transition in VO2: A view from the ultrafast timescale," *Physical Review B*, vol. 70, no. 16, pp. 1–4, 2004.

[33] P. Baum, D. S. Yang, and A. H. Zewail, "4D visualization of transitional structures in phase transformations by electron diffraction," *Science*, vol. 318, no. 5851, pp. 788–792, 2007.

[34] M. R. Bionta, V. Wanie, V. Gruson, J. Chaillou, N. Émond, D. Lepage, P. Lassonde, M. Chaker, and F. Légaré, "Probing the phase transition in VO2 using few-cycle 1.8 μm pulses," *Physical Review B*, vol. 97, no. 12, pp. 1–5, 2018.

[35] M. R. Otto, L. P. René de Cotret, D. A. Valverde-Chavez, K. L. Tiwari, N. Émond, M. Chaker, D. G. Cooke, and B. J. Siwick, "How optical excitation controls the structure and properties of vanadium dioxide," *Proceedings of the National Academy of Sciences of the United States of America*, vol. 116, no. 2, pp. 450–455, 2019.

[36] J. K. Clark, Y.-L. Ho, H. Matsui, B. Vilquin, H. Tabata, and J.-J. Delaunay, "Photo-induced metal-like phase of VO2 with sub-ns recovery," *ACS Photonics*, 2020.

[37] H. M. Wong, Z. Yan, K. A. Hallman, R. E. Marvel, R. P. Prasankumar, R. F. Haglund, and A. S. Helmy, "Broadband, Integrated, Micron-Scale, All-Optical Si3N4/VO2 Modulators with pJ Switching Energy," *ACS Photonics*, vol. 6, no. 11, pp. 2734–2740, 2019.

[38] A. Gil-Molina, I. Aldaya, J. L. Pita, L. H. Gabrielli, H. L. Fragnito, and P. Dainese, "Optical free-carrier generation in silicon nano-waveguides at 1550 nm," *Applied Physics Letters*, vol. 112, no. 25, 2018.

[39] Y. X. Ji, S. Y. Li, G. A. Niklasson, and C. G. Granqvist, "Durability of thermochromic VO2 thin films under heating and humidity: Effect of Al oxide top coatings," *Thin Solid Films*, vol. 562, pp. 568–573, 2014.

[40] T. Chang, X. Cao, N. Li, S. Long, Y. Zhu, J. Huang, H. Luo, and P. Jin, "Mitigating Deterioration of Vanadium Dioxide Thermochromic Films by Interfacial Encapsulation," *Matter*, vol. 1, no. 3, pp. 734–744, 2019.

[41] Y. Liu, J. Liu, Y. Li, D. Wang, L. Ren, and K. Zou, "Effect of annealing temperature on the structure and properties of vanadium oxide films," *Optical Materials Express*, vol. 6, no. 5, pp. 1552–1560, 2016.

[42] J. Y. Suh, R. Lopez, L. C. Feldman, and R. F. Haglund, "Semiconductor to metal phase transition in the nucleation and growth of VO2 nanoparticles and thin films," *Journal of Applied Physics*, vol. 96, no. 2, pp. 1209–1213, 2004.

[43] A. H. Atabaki, E. Shah Hosseini, A. A. Eftekhar, S. Yegnanarayanan, and A. Adibi, "Optimization of metallic microheaters for high-speed reconfigurable silicon photonics," *Optics Express*, vol. 18, no. 17, p. 18312, 2010.

[44] M. Bahadori, A. Gazman, N. Janosik, S. Rumley, Z. Zhu, R. Polster, Q. Cheng, and K. Bergman, "Thermal Rectification of Integrated Microheaters for Microring Resonators in Silicon Photonics Platform," *Journal of Lightwave Technology*, vol. 36, no. 3, pp. 773–788, 2018.

[45] J. Parra, J. Hurtado, A. Griol, and P. Sanchis, "Ultra-low loss hybrid ITO/Si thermo-optic phase shifter with optimized power consumption," *Optics Express*, vol. 28, no. 7, p. 9393, 2020.

[46] L. D. Sánchez, F. C. Juan, A. Rosa, and P. Sanchis, "Ultra-compact electro-absorption VO2-Si modulator with TM to TE conversion," *Journal of Optics (United Kingdom)*, vol. 19, no. 3, 2017.

[47] P. Xu, J. Zheng, J. K. Doylend, and A. Majumdar, "Low-Loss and Broadband Nonvolatile Phase-Change Directional Coupler Switches," *ACS Photonics*, vol. 6, no. 2, pp. 553–557, 2019.

[48] M. Miscuglio, G. C. Adam, D. Kuzum, and V. J. Sorger, "Roadmap on material-function mapping for photonic-electronic hybrid neural networks," *APL Materials*, vol. 7, no. 10, 2019.

[49] M. Miscuglio and V. J. Sorger, "Photonic tensor cores for machine learning," *Applied Physics Reviews*, vol. 7, no. 3, 2020.

[50] J. Feldmann, N. Youngblood, M. Karpov, X. Li, M. Stappers, M. Le Gallo, X. Fu, A. Lukashchuk, A. S. Raja, J. Liu, C. D. Wright, A. Sebastian, T. J. Kippenberg, W. H. P. Pernice, and H. Bhaskaran, "Parallel convolutional processing using an integrated photonic tensor core," *Nature*, vol. 589, no. January, pp. 52–58, 2021.